Seatific, Vol. 3, Issue. 1, pp. 9–18, June 2023

Seatific Journal
https://seatific.yildiz.edu.tr
DOI: https://doi.org/10.14744/seatific.2023.0002

Research Article

Optimizing the power of a variable-temperature heat reservoir Brayton cycle for a nuclear power plant in space

Tan WANG[1,2,3], Lingen CHEN*[1,2,3], Yanlin GE[1,2,3], Shuangshuang SHI[1,2,3], Huijun FENG[1,2,3]

[1]*Institute of Thermal Science and Power Engineering, Wuhan Institute of Technology, Wuhan, China*
[2]*Hubei Provincial Engineering Technology Research Center of Green Chemical Equipment, Wuhan, China*
[3]*School of Mechanical & Electrical Engineering, Wuhan Institute of Technology, Wuhan, China*

ARTICLE INFO

Article history
Received: March 22, 2023
Revised: May 5, 2023
Accepted: May 8, 2023

Key words:
Endoreversible closed Brayton cycle; finite time thermodynamics; optimal performance; power optimization; space power plant; variable-temperature heat reservoir cycle

ABSTRACT

This study establishes a variable-temperature heat reservoir endoreversible simple closed Brayton cycle model for a nuclear power plant in space and derives its thermal efficiency (TEF) and power output (POW). The maximum POW (P_{max}) for a fixed total heat transfer area of a radiator panel and two heat exchangers (HEXs) is obtained by optimizing the area distributions (f_H, f_L, and f_R) among the two HEXs and radiator panel, the double maximum POW ($P_{max,2}$) is obtained by optimizing the inlet temperature ($T_{L_{in}}$) of the cooling fluid in the low temperature heat sink, and the triple maximum POW ($P_{max,3}$) is further obtained by optimizing the thermal capacity rate matching (C_{Wf}/C_H) between the heat reservoir and working fluid. When f_H, f_L, and f_R, are optimized, P_{max} increases by 4.33% compare to the initial POW (P); when T_{Lin} is furtherly optimized, $P_{max,2}$ increases by 6.33% compare to P and increases by 1.86% compared to P_{max}, with $P_{max,3}$ increasing by 11.76%, 7.13%, and 5.17% compared to P, P_{max}, and $P_{max,2}$, respectively.

Cite this article as: Wang T, Chen L, Ge Y, Shi S, Feng H. Optimizing the power of a variable-temperature heat reservoir Brayton cycle for a nuclear power plant in space. Seatific 2023;3:1:9–18.

1. INTRODUCTION

In the face of the requirements of deep space exploration missions, establishing a high-conversion efficiency, reliable, and compact space-based power plant (SPP) that can respond to challenges has become necessary in recent years. Three ways presently exist for an SPP to provide energy: chemical, solar, or nuclear energy. Among these options, nuclear energy appears as a possible alternative for generating large amounts of energy long term and reducing fuel mass. Furthermore, the SPP would require the maximum power-to-mass ratio for space propulsion purposes. Therefore, a practical energy conversion system must strike a compromise between high conversion efficiency and compactness. This relationship must be balanced during the design process. The main components of SPP are divided into three parts: the reactor, the energy conversion device, and the radiator. The space energy conversion system can be separated into static (thermoelectric converter and thermionic conversion) and dynamic (Stirling, Brayton, and Rankine heat engines) components.

Due to the high power density, high conversion efficiency, stability, and reliability, the closed Brayton cycle and its combined cycles have been used in aircraft, the marine industry, power plants, and space-based power plants. Some scholars (Gonca & Sahin, 2016; Gonca, 2017a, 2017b, 2018; Gonca & Genc, 2019;Gonca & Başhan, 2019; Gonca & Guzel, 2022) have optimized gas turbine cycles

***Corresponding author.**
*E-mail address: lingenchen@hotmail.com, 2506715339@qq.com

(Gonca & Sahin, 2016; Gonca, 2017a, 2018), gas-mercury cycles (Gonca, 2017b; Gonca & Genc, 2019) and gas-steam combined cycles (Gonca & Başhan, 2019; Gonca & Guzel, 2022) with exergetic (Gonca, 2017a, 2017b; Gonca & Guzel, 2022), exergo-economic (Gonca & Guzel, 2022) and thermo-ecological (Gonca & Sahin, 2016; Gonca, 2017a, 2017b, 2018; Gonca & Genc, 2019;Gonca & Başhan, 2019) performances as the optimization objectives and analyzed the effects of different working fluids, turbine operations, and design parameters on cycle performances.

In order to establish a high conversion efficiency, reliable, and compact SPP, some scholars have introduced classical thermodynamics theory into the performance optimization of the closed Brayton cycle for SPPs (El-Genk & Tournier, 2009; Liu et al., 2020; Wang et al., 2021a; Miao et al., 2022; Toro & Lior, 2017). El-Genk and Tournier (2009) established a closed Brayton cycle model for SPP with an inert gas and binary mixture as a coolant and analyzed the influence of the working fluid (WF) on plant performance and turbine size. Their results showed that a cycle with an indirect closed Brayton cycle has higher thermal efficiency (TEF) than one with a single compressor and that the cycle TEF is almost unaffected by the WF's molecular weight. Liu et al. (2020) took the mass of the HEXs of a closed Brayton cycle for an SPP as the optimization objective, minimizing the total mass of the plant by optimizing the key parameters of the system components with NSGA-II algorithm, thus obtaining a Pareto frontier of key parameters. Wang et al. (2021a) established a closed Brayton cycle model for an SPP with a gas-cooled reactor as the hot side of the heat reservoirs (HRs) and analyzed and optimized the cycle performances. Their results showed the highest temperature that the fuel can reach and how safe the device is under optimal operation. Miao et al. (2022) established a recompressed supercritical N_2O-He mixture closed Brayton cycle model for an SPP. They comprehensively studied and optimized important parameters of the plant such as split ratio and pressure ratio and obtained an optimal TEF and closed Brayton cycle rotating unit mass for the cycle. Additionally, Toro and Lior (2017) introduced classical thermodynamics theory into the performance optimization of Stirling cycles for SPPs and analyzed the effects of main cycle parameters on the relationship between TEF and POW for Stirling cycles operating with different WFs.

The theory of finite-time thermodynamics (FTT; Andresen, 1983; Bejan, 1996; Chen et al. 1999; Berry et al., 2020; Andresen & Salamon, 2022) is an innovation of classical thermodynamic theory. FTT can consider the effects of heat transfer loss and the limitations of time and heat exchanger (HEX) area between the heat reservoir (HR) and WF which are largely ignored in classical thermodynamics. Many researchers have introduced FTT into the performance optimizations of thermal cycles and processes, including the optimal performances of the Carnot cycles (Curzon & Ahlborn, 1975; Valencia-Ortega et al., 2021), Stirling engines (Xu et al., 2022), diesel engines (Wu, Feng et al., 2021; Ge et al., 2021), dual cycles (Ge et al., 2022), Kalina cycles (Feng et al., 2020), dual-Miller cycles (Ebrahimi, 2021), organic Rankine cycles (Park & Kim, 2016; Wu, Ge et al., 2020; Feng et al., 2021), combined cycles (Gonca & Guzel, 2022; Wu et al., 2021), thermoelectric devices (Chen et al., 2020a; Chen et al., 2021a; Chen & Lorenzini, 2022a), thermal Brownian cycles (Qi et al., 2021a, 2021b; Chen et al., 2022; Qi et al., 2022a, 2022b), thermoradiative devices (Li & Chen, 2021; Zhang, Yang et al. 2021), blue engines (Lin et al., 2022), electron engines (Ding et al., 2021; Qui et al., 2021a), thermionic devices (Qiu et al., 2021b), methane reforming (Chen et al., 2022b), chemical engines (Chen & Xia, 2022a, 2023a), chemical pumps (Chen et al., 2023a, 2023b), Brayton cycles (Ibrahim et al., 1991; Ust et al., 2006; Chen et al. 2020b, 2020c; Qui et al., 2022; Jin et al, 2022), and refrigeration cycles (Chen & Lorenzini, 2022b), as well as the optimal configurations of refrigeration cycles (Badescu, 2021; Paul & Hoffman, 2022), heat-transfer systems (Badescu, 2022; Chen & Xia, 2022b), variable-temperature-reservoir heat engines (Li & Chen, 2022; Chen & Xia, 2022c), methanol synthesis (Li et al., 2022), variable-potential-reservoir chemical engines (Chen & Xia, 2022d, 2022e, 2023b, 2023c), and commercial engines (Chen, 2011; Chen & Xia, 2022f). Thermal cycles are divided into two types based on the nature of the cycle: steady flow cycles (Chen et al., 1996; Feidt, 2017) and reciprocating cycles (Curzon & Ahlborn, 1975; (Muschik & Hoffman, 2020). For the steady-flow heat engine cycle, considering the variable-temperature HR can have the cycle more closely approach the working state of actual heat engines. Therefore, some scholars have studied the steady-flow cycle under the condition of variable-temperature HRs (Ust et al., 2006; Ibrahim & Bourisli, 2021).

Some scholars have introduced FTT into the performance optimization of Stirling and Carnot engine cycles for SPPs (de Moura et al., 2022a, 2022b; Wang et al., 2021b, 2022). De Moura et al. (2022a, 2022b) established a Stirling engine model for an SPP, obtained a compact system with optimal temperature conditions for TEF by optimizing the temperature of the HRs of the system, and analyzed different the effects of the Stirling engine structural parameters on final system performance. Wang et al. (2021b, 2022) respectively established endoreversible and irreversible Carnot cycle models for SPPs and obtained the plant double-maximum POW by optimizing the area distributions of the HEXs and temperature of the low temperature heat sink.

Some scholars (Zhang, Liu et al., 2021; Romano & Ribiero, 2021) introduced FTT into the performance optimizations of a closed Brayton cycle for SPPs. Zhang, Liu et al. (2021) established a supercritical CO2 closed Brayton cycle model for an SPP using a sodium-cooled reactor as the hot side of the HR, derived the relationship between TEF and POW, and obtained optimal cycle characteristics and operating parameters. Romano and Ribeiro (2021) established a regenerative closed Brayton cycle model for an SPP, obtained the optimal inlet temperature for the cold side of the HEX and optimal heat source temperature by minimizing specific mass.

Existing FTT research on closed Brayton cycle models for SPPs have not optimized HEX area or HR temperature, nor have they yet obtained the optimal inlet temperature of a cooling fluid in a low temperature heat sink or optimize thermal capacity rate matching between the HR and WF. Applying FTT to SPPs is crucial for establishing a theoretical system, and based on Ust et al. (2006), this paper will establish a variable temperature HR endoreversible closed Brayton cycle model for an SPP. For a fixed total heat transfer area of the radiator panel and two HEXs, the maximum POW of the plant will be obtained by optimizing the area distributions among the radiator panel and two HEXs, the double-maximum POW will be obtained by optimizing the inlet temperature of the cooling fluid in the low temperature heat sink, and the triple-maximum POW will be obtained by optimizing thermal capacity rate matching between the HR and WF. The study will also investigate the impacts the cycle parameters have on the triple-maximum POW.

2. MODEL DESCRIPTION AND PERFORMANCE INDICATORS

Figure 1 shows the diagram of the established model. The model consists of two parts: the first part is the ordinary closed Brayton cycle, which includes a compressor, a turbine, and two HEXs between the HRs and WF. This part has isobaric heat absorption and heat release processes involving the temperature drops T_3-T_2 accompanying Q_H and T_4-T_1 accompanying Q_L (denoted respectively as the processes 2→3 and 4→1 in Fig. 1). This part also undergoes two isentropic processes (denoted as processes 1→2 and 3→4 in Fig. 1). The second part includes a radiator panel that dissipates heat into space. The HEXs between the HRs and WF are assumed to be counter-current. The inlet/outlet temperatures of the heating and cooling fluids are T_{Hin}/T_{Hout} and T_{Lin}/T_{Lout}, respectively.

The constant thermal capacity rate of the WF is C_{wf}, and the thermal capacity rates of the HRs are C_H and C_L. The heat conductance of the hot and cold sides of the HEX are U_H and U_L. $U_H=K_1F_H$ and $U_L=K_2F_L$, where K is the heat transfer coefficient and F is the HEX area.

According to the properties of the WF and HEX theory, the heat flux between the HRs and WF are respectively:

$$Q_H=C_{wf}(T_3-T_2)=C_{H\,min}E_{H1}(T_{Hin}-T_2) \quad (1)$$

$$Q_L=C_{wf}(T_4-T_1)=C_{L\,min}E_{L1}(T_4-T_{Lin}) \quad (2)$$

where the Es are the effectiveness values of the two HEXs:

$$E_{H1}=\frac{1-\exp[-N_{H1}(1-C_{H\,min}/C_{H\,max})]}{1-(C_{H\,min}/C_{H\,max}\exp[-N_{H1}(1-C_{H\,min}/C_{H\,max})]} \quad (3)$$

$$E_{L1}=\frac{1-\exp[-N_{L1}(1-C_{L\,min}/C_{L\,max})]}{1-(C_{L\,min}/C_{L\,max}\exp[-N_{L1}(1-C_{L\,min}/C_{L\,max})]} \quad (4)$$

$$N_{H1}=U_H/C_{H\,min}=K_1F_H/C_{H\,min},\ N_{L1}=U_L/C_{L\,min}/C_{L\,max})] \quad (5)$$

$$C_{H\,max}=max\{C_H, C_{wf}\},\ C_{H\,min}=min\{C_H, C_{wf}\} \quad (6)$$

$$C_{L\,max}=max\{C_L, C_{wf}\},\ C_{L\,min}=min\{C_L, C_{wf}\} \quad (7)$$

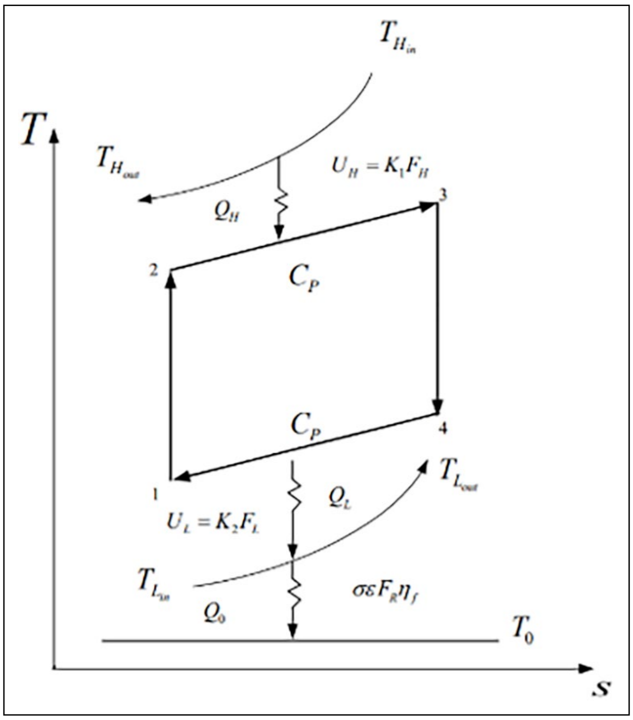

Figure 1. The *T-s* diagram of a variable temperature HR endoreversible closed Brayton cycle for an SPP.

HR: Heat reservoir; SPP: Space power plant.

where $C_{H\,max}$ and $C_{H\,min}$ are the respective maximum and minimum thermal capacity rates regarding C_{wf} and C_H, $C_{L\,max}$ and $C_{L\,min}$ are the respective maximum and minimum thermal capacity rates regarding C_{wf} and C_L, and N_{H1} and N_{L1} are the respective number of heat transfer units as defined based on the minimum thermal capacity.

According to the endoreversible condition, the relationship between the four temperatures of the cycle is $T_1T_3=T_2T_4$. Defining the isentropic temperature ratio of the compressor as x gives:

$$x=\frac{T_2}{T_1}=\frac{T_3}{T_4}=\left(\frac{P_2}{P_1}\right)^m=\pi^m \quad (8)$$

where π is the pressure ratio of the cycle, $m=(k-1)/k$, and k is the specific heat ratio.

The steady-state heat transfer from the radiator panel to the external environment is:

$$Q_0=\sigma\varepsilon F_R\eta_f(T_{Lin}^4-T_0^4) \quad (9)$$

where η_f is fin efficiency, σ is the Boltzmann constant, T_0 is the temperature of the space environment, ε is emissivity, and F_R is the area of the radiator panel.

According to Ust et al. (2006), outlet temperatures T_2 and T_4 of the compressor and turbine for a conventional variable temperature HR endoreversible closed Brayton cycle model are obtained as:

$$T_2=\frac{C_{H\,min}E_{H1}(C_{wf}-C_{L\,min}E_{L1})T_{Hin}+xC_{wf}C_{L\,min}E_{L1}T_{Lin}}{C_{wf}^2/C_{wf}-C_{H\,min}E_{H1})(C_{wf}-C_{L\,min}E_{L1})} \quad (10)$$

$$T_4=\frac{x^{-1}C_{H\,min}E_{H1}C_{wf}T_{Hin}+C_{L\,min}E_{L1}(C_{wf}-C_{H\,min}E_{H1})T_{Lin}}{C_{wf}^2/C_{wf}-C_{H\,min}E_{H1})(C_{wf}-C_{L\,min}E_{L1})} \quad (11)$$

From the first law of thermodynamics, one can obtain:

$$Q_L=Q_0 \tag{12}$$

$$C_{L\,min}\,E_{L1}\,(T_4\text{-}T_{Lin})=\sigma\varepsilon F_R\eta_f\,(T^4_{Lin}\text{-}T^4_0) \tag{13}$$

From Eqs. 11 and 13, one gets:

$$T_4=\frac{\sigma\varepsilon F_R\eta_f\,(T^4_{Lin}\text{-}T^4_0)}{C_{L\,min}\,E_{L1})} \tag{14}$$

$$\frac{\sigma\varepsilon F_R\eta_f\,(T^4_{Lin}\text{-}T^4_0)}{(C_{L\,min}\,E_{L1})}+T_{Lin}= \frac{x^{-1}\,C_{H\,min}\,E_{H1}\,C_{wf}\,T_{Hin}+C_{L\,min}\,E_{L1}\,(C_{wf}\text{-}C_{H\,min}\,E_{H1})\,T_{Lin}}{C_{wf}^{\,2}/C_{wf}\text{-}C_{H\,min}\,E_{H1})\,(C_{wf}\text{-}C_{L\,min}\,E_{L1})} \tag{15}$$

From Eq. 15, one then gets:

$$x=\pi^m=(C_{H\,min}\,E_{H1}\,C_{wf}\,T_{Hin})/\{[((C_{wf}^{\,2}\text{-}(C_{wf}\text{-}C_{H\,min}\,E_{H1})\,(\mathrm{C_{wf}}\text{-}\mathrm{C_{L\,min}}\,\mathrm{E_{L1}}))] \\ [(\frac{\sigma\varepsilon F_R\eta_f\,(T^4_{Lin}\text{-}T^4_0)}{(C_{L\,min}\,E_{L1})}+T_{Lin})\text{-}C_{L\,min}\,E_{L1}\,(C_{wf}\text{-}C_{H\,min}\,E_{H1})\,T_{Lin})]\} \tag{16}$$

From Eqs. 10 and 16, one gets:

$$T_2=[(((C_{wf}^{\,2}\text{-}(C_{H\,min}\,E_{H1}(C_{wf}\text{-}C_{L\,min}\,E_{L1})\,T_{Hin}\,C_{wf}^{\,2}\text{-}(C_{wf}\text{-}C_{H\,min}\,E_{H1})) \\ +(C_{H\,min}\,E_{H1}\,C_{wf}\,T_{Hin}+C_{L\,min}\,E_{L1}\,(C_{wf}\text{-}C_{H\,min}\,E_{H1})T_{Lin})C_{wf}C_{L\,min}E_{L1}T_{Lin}))] \\ /[(((C_{wf}\text{-}C_{H\,min}\,E_{H1})(C_{wf}\text{-}C_{L\,min}\,E_{L1}))(C_{wf}\text{-}C_{L\,min}E_{L1})(\frac{\sigma\varepsilon F_R\eta_f\,(T^4_{Lin}\text{-}T^4_0)}{(C_{L\,min}\,E_{L1})}+T_{Lin}))] \tag{17}$$

From Eqs. 1, 2, 14, and 17, one then gets:

$$Q_H=[(C_{H\,min}\,E_{H1}(T_{Hin}\text{-}((C_{wf}^{\,2}\text{-}(C_{H\,min}\,E_{H1}(C_{wf}\text{-}C_{L\,min}\,E_{L1})T_{Hin}C_{wf}^{\,2}\text{-}(C_{wf}\text{-}C_{H\,min}\,E_{H1})) \\ +(C_{H\,min}\,E_{H1}\,C_{wf}\,T_{Hin}+C_{L\,min}\,E_{L1}\,(C_{wf}\text{-}C_{H\,min}\,E_{H1})T_{Lin})C_{wf}C_{L\,min}E_{L1}T_{Lin})))] \\ /[(((C_{wf}\text{-}C_{H\,min}\,E_{H1})(C_{wf}\text{-}C_{L\,min}\,E_{L1}))(C_{wf}\text{-}C_{L\,min}E_{L1})(\frac{\sigma\varepsilon F_R\eta_f\,(T^4_{Lin}\text{-}T^4_0)}{(C_{L\,min}\,E_{L1})}+T_{Lin}))] \tag{18}$$

$$Q_L=C_{L\,min}\,E_{L1}\frac{\sigma\varepsilon F_R\eta_f\,(T_{Lin}^{\;4}\text{-}T_0)^4}{C_{L\,min}\,E_{L1})} \tag{19}$$

Thus, the POW and TEF of the plant are respectively:

$$P=Q_H\text{-}Q_L=\{[C_{H\,min}\,E_{H1}(T_{Hin}\text{-}((C_{wf}^{\,2}\text{-}(C_{H\,min}\,E_{H1}(C_{wf}\text{-}C_{L\,min}\,E_{L1})T_{Hin}C_{wf}^{\,2}\text{-}(C_{wf}\text{-}C_{H\,min}\,E_{H1})) \\ +(C_{H\,min}\,E_{H1}\,C_{wf}\,T_{Hin}+C_{L\,min}\,E_{L1}\,(C_{wf}\text{-}C_{H\,min}\,E_{H1})T_{Lin})C_{wf}C_{L\,min}E_{L1}T_{Lin}))] \\ /[(((C_{wf}\text{-}C_{H\,min}\,E_{H1})(C_{wf}\text{-}C_{L\,min}\,E_{L1}))(C_{wf}\text{-}C_{L\,min}E_{L1})(\frac{\sigma\varepsilon F_R\eta_f\,(T^4_{Lin}\text{-}T^4_0)}{(C_{L\,min}\,E_{L1})}+T_{Lin}))]\} \\ \text{-}(C_{L\,min}\,E_{L1}\frac{\sigma\varepsilon F_R\eta_f\,(T^4_{Lin}\text{-}T^4_0)}{C_{L\,min}\,E_{L1})} \tag{20}$$

$$\eta=1\text{-}(Q_H/Q_L)=1\text{-}\{\{[(C_{H\,min}E_{H1}\,(T_{Hin}\text{-}((C_{wf}^{\,2}\text{-}(C_{H\,min}E_{H1} \\ \times(C_{wf}\text{-}C_{L\,min}\,E_{L1})T_{Hin}C_{wf}^{\,2}\text{-}(C_{wf}\text{-}C_{H\,min}E_{H1})) \\ /[(C_{wf}\text{-}C_{H\,min}\,E_{H1})(C_{wf}\text{-}C_{L\,min}\,E_{L1}))(C_{wf}\text{-}C_{L\,min}E_{L1})(\frac{\sigma\varepsilon F_R\eta_f\,(T^4_{Lin}\text{-}T^4_0)}{(C_{L\,min}\,E_{L1})}+T_{Lin})]\} \\ /[C_{L\,min}\,E_{L1}\frac{\sigma\varepsilon F_R\eta_f\,(T^4_{Lin}\text{-}T^4_0)}{(C_{L\,min}\,E_{L1})}]\} \tag{21}$$

3. POWER MAXIMIZATION

3.1. Initial design

In accordance with Ust et al. (2006), Wang et al. (2021b, 2022), and Romano & Ribiero (2021), an initial design has been performed with σ=5.67×10^{-11}kW/(m^2·K^4), η_f=0.9, ε=0.9, C_{wf}=1.5kW/K, C_L=C_H=1.2kW/K, K_1=K_2=0.2kW/(m^2·L), T_{Hin}=1150K, T_{Lin}=400K, T_0=200K, F_H=12.24m^2, F_L=12.24m^2, and F_R=122.4m^2. The POW of the initial design is P=122.94.

3.2. The maximum and double-maximum POWs

A change in the area of the HEXs will also change and, thus enabling the POW to be maximized. Assuming that the sum of the area of the three HEXs is constant:

$$F_H+F_L+F_R=F_T \tag{22}$$

and defining the three area distribution ratios as:

$$f_i=F_i/F_T\ (i=H,\ L,R) \tag{23}$$

$$\sum f_i=1,\ 0<f_i<1\ (i=H,\ L,\ R) \tag{24}$$

one can perform the POW maximization with respect to the area ratios. The obtained maximum POW is P_{max} .

Figure 2 reflects P versus f_H and f_L with F_T=153.8 m^2, C_{wf}=1.5kW/K, K_1=K_2=0.2kW/(m^2·K), T_{Hin}=1150K, T_{Lin}=400K, C_L=C_H=1.2kW/K, and T_0=200K. $P_{\max}$ (the peak of the curve in Fig. 3) is obtained with HEXs' area allocations f_H and f_L as optimization variables and the fixed F_T, with the corresponding optimal area allocations of the HEXs and radiator panel being f_{Hopt}, f_{Lopt}, and f_{Ropt}, respectively. $P_{\max}$ is 128.26kW, with $P_{\max}$ increasng by about 4.33% compared to the POW (P) of the initial design.

The double-maximum POW ($P_{\max,2}$) is further obtained by optimizing the inlet temperature of the cooling fluid (T_{Lin}) based on f_{Hopt}, f_{Lopt}, and f_{Ropt}. Figure 3 reflects the maximum POW ($P_{\max}$) versus T_{Lin}. In the calculation, almost all of the parameters are the same as those for Figure 2 except T_{Lin}, which is variable. $P_{\max,2}$ (the peak of the curve in Fig. 3) is 130.65 ; with $P_{\max,2}$ increasing by about 1.86% compared to maximum POW ($P_{\max}$), and $P_{\max,2}$ increasing by about 6.27% compared to the POW (P) of the initial design.

Here the study will perform some parameter analyses regarding the maximum POW and double-maximum POW. Figures 4 and 5 reflect the effects of the thermal capacity rate (C_{wf}) of the WF and heat transfer coefficients of the HEXs (K_1 and K_2) on the relationship between $P_{\max}$ and the corresponding TEF (η_{opt}), the relationship between $P_{\max}$ and the inlet temperature of the cooling fluid (T_{Lin}), the relationship between $P_{\max}$ and f_{Hopt} (f_{Ropt}), as well as the relationship between $P_{\max}$ and the corresponding pressure ratio (π).

Figure 4 reflects $P_{\max}$-T_{Lin}, $P_{\max}$-η_{opt}, $P_{\max}$-f_{Hopt}, $P_{\max}$-f_{Ropt}, and $P_{\max}$-π under different C_{wf} values. When K_1=K_2=0.2kW/(m^2·K), increasing C_{wf} also increases the TEF [(η_{opt}) $P_{\max,2}$], radiator area allocation [(f_{Ropt}) $P_{\max,2}$], and pressure ratio [(π_{opt}) $P_{\max,2}$] at double-maximum POW ($P_{\max,2}$) while decreasing $P_{\max,2}$, the hot side of the HEX area allocation [(f_{Hopt}), $P_{\max,2}$], and the inlet temperature of the cooling fluid [(T_{Lin}) $P_{\max,2}$] at $P_{\max,2}$. C_{wf} values of 1.5, 2.0, and 2.5 result in respective $P_{\max,2}$ values of 130.65 kW, 126.33 kW, and 123.042

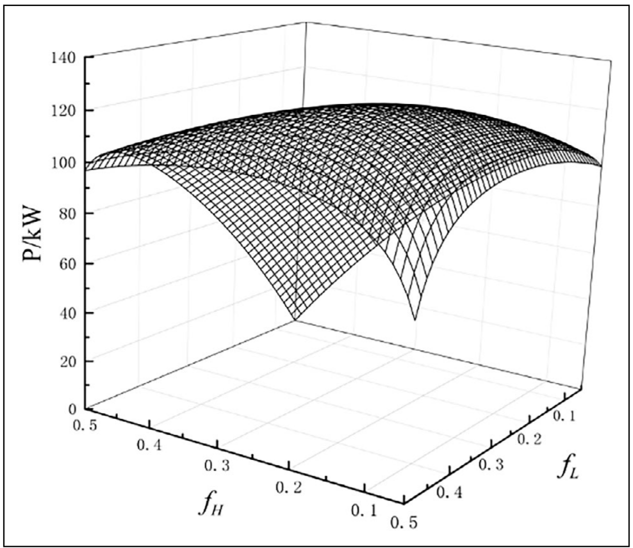

Figure 2. The relations of P versus f_H and f_L.

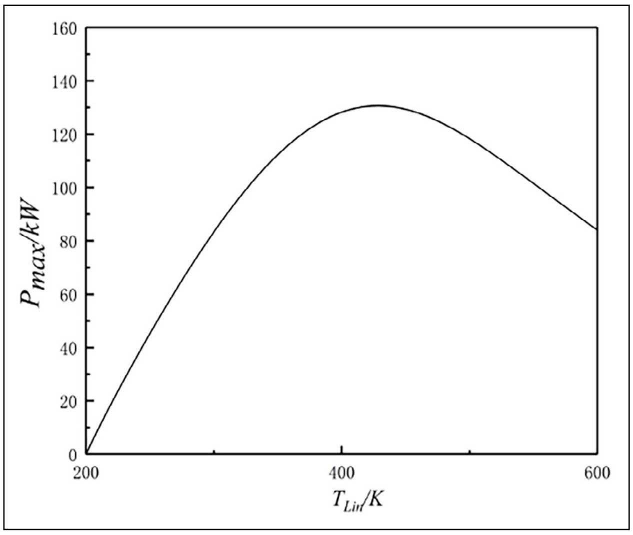

Figure 3. The relations of $P_{\max}$ versus T_{Lin}.

kW; respective (T_{Lin}) $P_{\max,2}$ values of 428 K, 419 K, and 413 K; respective values of 0.468, 0.473, and 0.476, respective (η_{opt}) $P_{\max,2}$ values of 9.10, 9.41, and 9.59; respective (f_{Hopt}) $P_{\max,2}$ values of 0.171, 0.156, and 0.151; and respective (f_{Ropt}) $P_{\max,2}$ values of 0.658, 0.68, and 0.698. Increasing C_{wf} from 1.5 to 2.5 decreases $P_{\max,2}$ by about 5.82% and (T_{Lin}) $P_{\max,2}$ by about 3.50%, increases (η_{opt}) $P_{\max,2}$ by about 1.71%, decreases (f_{Hopt}) $P_{\max,2}$ by about 11.70%, and increases (f_{Ropt}) $P_{\max,2}$ by about 5.71% as well as (π_{opt}) $P_{\max,2}$ by about 5.49%.

The optimal pressure ratio ((π_{opt}) $P_{\max,2}$) corresponding to $P_{\max,2}$ should be pointed out to have one-to-one correspondence to the optimal inlet temperature of the cooling fluid [(T_{Lin}) $P_{\max,}$]; namely, only one independent variable is found between the inlet temperature of the cooling fluid (T_{Lin}) and the pressure ratio (π).

Figure 5 reflects the $P_{\max}$-T_{Lin}, $P_{\max}$-η_{opt}, $P_{\max}$-f_{Hopt}, $P_{\max}$-f_{Ropt} and $P_{\max}$-π values under different K_1=K_2 and. When C_{wf}=1.5, increases to K_1 and K_2 will increase $P_{\max,2}$, (T_{Lin}) $P_{\max,2}$, and (f_{Ropt}) $P_{\max,2}$ while decreasing (f_{Hopt}), $P_{\max,2}$, and (η_{opt}) $P_{\max,2}$. When K_1 and K_2 are 0.1, 0.2, and 0.3, $P_{\max,2}$ has respective values of 111.94kW, 130.65kW, and 139.75kW; (T_{Lin}) $P_{\max,2}$ has respective values of 426 K, 428 K, and 429.8 K; (η_{opt}) $P_{\max,2}$ has respective values of 0.469, 0.468, and 0.467; (π_{opt}) $P_{\max,2}$ has respective values of 9.15, 9.10, and 9.08; (f_{Hopt}), $P_{\max,2}$ has respective values of 0.213, 0.171, and 0.147; and (f_{Ropt}), $P_{\max,2}$ has respective values of 0.573, 0.658, and 0.706. Increasing K_1 and K_2 from 0.1 to 0.3 increases $P_{\max,2}$ by about 24.84% and (T_{Lin}) $P_{\max,2}$ by about 0.89%, decreases (η_{opt}) $P_{\max,2}$ by about 0.426% and (f_{Hopt}), $P_{\max,2}$ by about 30.99%, increases (f_{Ropt}), $P_{\max,2}$ by about 23.21%, and decreases (π_{opt}) $P_{\max,2}$ by about 0.765%.

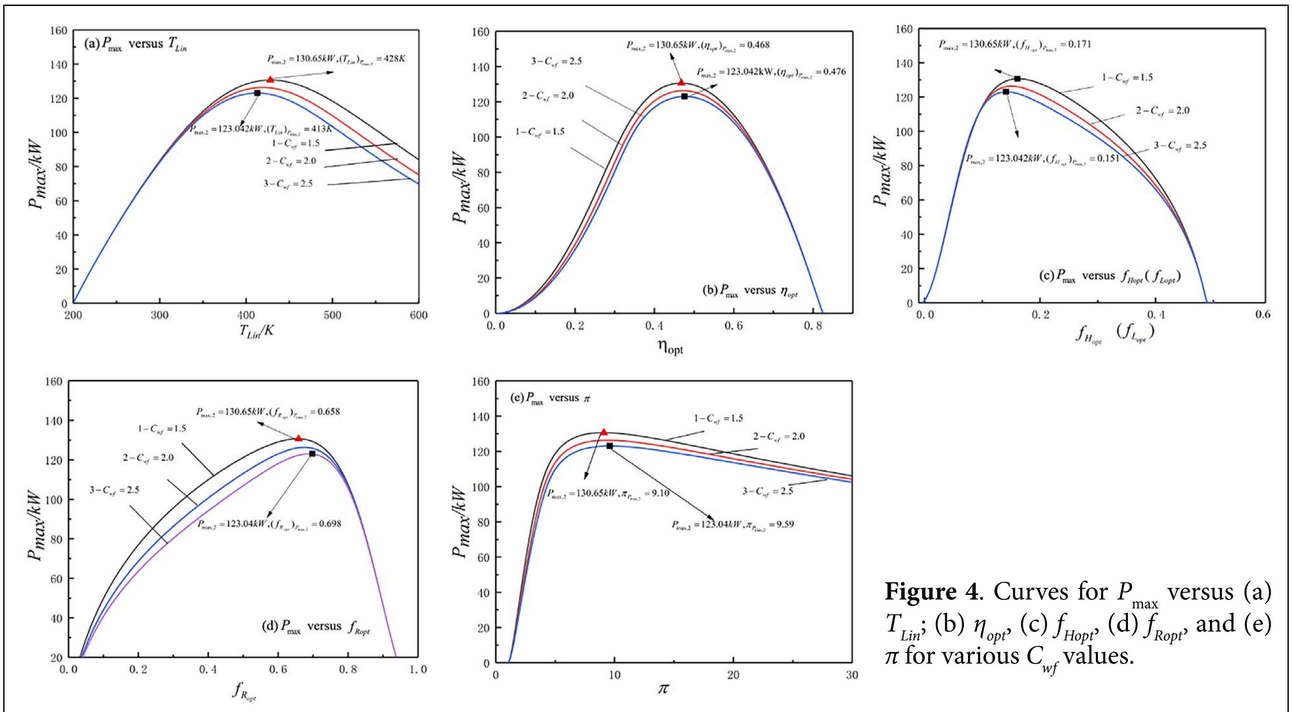

Figure 4. Curves for $P_{\max}$ versus (a) T_{Lin}; (b) η_{opt}, (c) f_{Hopt}, (d) f_{Ropt}, and (e) π for various C_{wf} values.

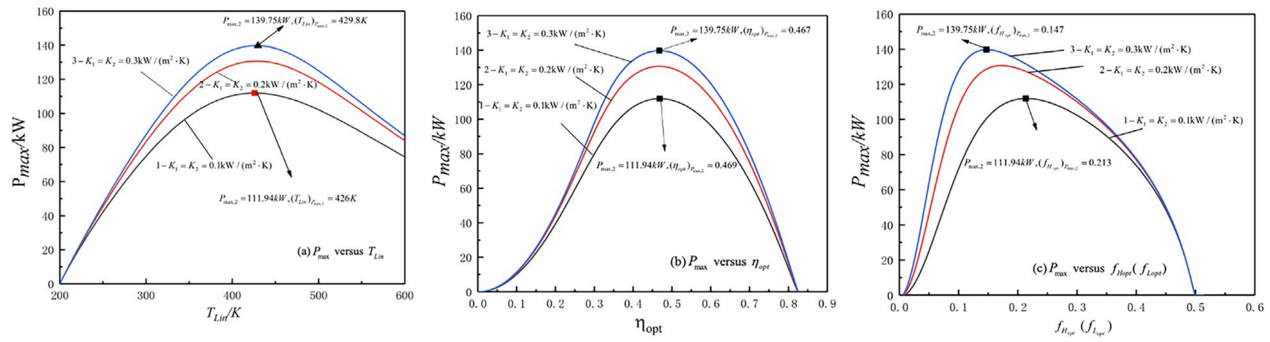

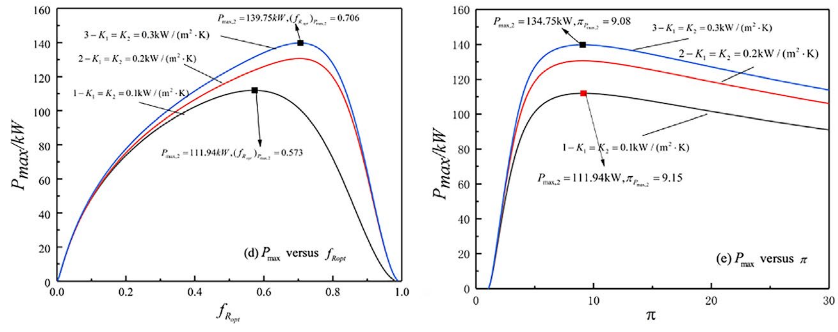

Figure 5. Curves for P_{max} versus (a) T_{Lin}; (b) η_{opt}, (c) f_{Hopt}, (d) f_{Ropt}, and (e) π for different K_1 and K_2 values.

3.3. The triple-maximum POW

The triple maximum POW ($P_{max,3}$) has been further obtained by optimizing the thermal capacity rate matching (C_{wf}/C_H) between the HRs and WF based on f_{Hopt}, f_{Lopt}, f_{Ropt}, and (T_{Lin}) $P_{max,2}$. When almost all of the parameters are the same as those for Figure 3 except for C_{wf}/C_H, which is variable, the optimization shows the triple maximum POW to be $P_{max,3}$=137.40 kW, as shown by the peak of Curve 2 in Figure 6. $P_{max,3}$ increases by about 5.17% compared to the double-maximum POW ($P_{max,2}$), by about 7.13% compared to the maximum POW (P_{max}), and by about 11.76% compared to the POW (P) of the initial design.

Now we further study the effects of the thermal capacity ratio (C_L/C_H) of the HRs and K_1 on the triple-maximum POW ($P_{max,3}$). Figures 6 and 7 reflect $P_{max,2}$-C_{wf}/C_H under different C_L/C_H and K_1 values, respectively. One can see that as C_{wf}/C_H increases, $P_{max,2}$-C_{wf}/C_H reflects a stable parabolic-like change, and an optimal C_{wf}/C_H [$(C_{wf}/C_H)_{opt}$] is found for the cycle to reach triple-maximum POW ($P_{max,3}$; i.e., the peaks of the curves).

Figure 6 reflects $P_{max,2}$-C_{wf}/C_H under different C_L/C_H. When K_1=K_2=0.2kW/(m²·K), increasing C_L/C_H increases both $P_{max,3}$ and $(C_{wf}/C_H)_{opt}$. C_L/C_H values of 0.6, 1.0, and 1.6 result in respective $P_{max,3}$ values of 116.57, 137.40, and 148.31 kW and corresponding $(C_{wf}/C_H)_{opt}$ values of 0.75, 1.0, and 1.23. When C_L/C_H increases from 0.6 to 1.6, $P_{max,3}$ increases by about 27.23%, while $(C_{wf}/C_H)_{opt}$ increases by about 64%.

Figure 7 reflects the $P_{max,2}$-C_{wf}/C_H curve for different K_1 values. When K_2=0.2kW/(m²·K) and C_L/C_H=*1.6*, increasing K_1 results in $P_{max,3}$ increasing and $(C_{wf}/C_H)_{opt}$ decreasing. For K_1 values of 0.2, 0.3, and 0.4, $P_{max,3}$ has respective values of 148.31, 153.95, and 157.38 kW and corresponding $(C_{wf}/C_H)_{opt}$ values of 1.23, 1.20, and 1.18. When K_1 increases from 0.2 to 0.4, $P_{max,3}$ increases by about 6.12%, while $(C_{wf}/C_H)_{opt}$ decreases by about 4.07%.

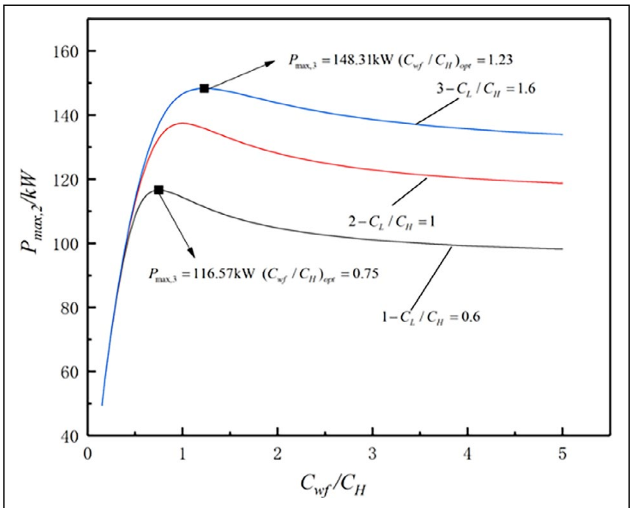

Figure 6. $P_{max,2}$ versus C_{wf}/C_H for different C_L/C_H values.

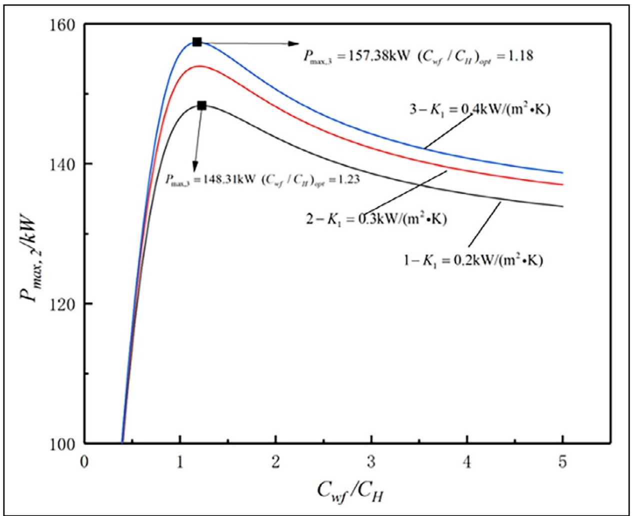

Figure 7. $P_{max,2}$ versus C_{wf}/C_H for different K_1 values.

4. CONCLUSION

Based on Ust et al. (2006), this study has established a variable temperature HR endoreversible closed Brayton cycle for an SPP and derived the relationships between POW (P) and inlet temperature of the cooling fluid in a low temperature heat sink, as well as between the TEF and inlet temperature of the cooling fluid. For a fixed total heat transfer area of two HEXs and one radiator panel, the maximum POW ($P_{\max}$) of the plant is obtained by optimizing the area distributions (f_H, f_L, and f_R) among the two HEXs and the radiator panel; the double-maximum POW ($P_{\max,2}$) is obtained by optimizing the inlet temperature of the cooling fluid (T_{Lin}), and the triple-maximum POW ($P_{\max,3}$) is further obtained by optimizing the thermal capacity rate matching (C_{wf}/C_H) between the HRs and WF. The optimization effects are obvious. This study has researched the impacts of plant parameters on optimal performance, and the main conclusions are as follow:

1. Optimal f_{Hopt}, f_{Lopt} and f_{Ropt} values exist for having the cycle reach $P_{\max}$. Optimal T_{Lin} and optimal f_{Hopt}, f_{Lopt} and f_{Ropt} values exist for having the cycle reach $P_{\max,2}$. The curve $P_{\max,2}$-C_{wf}/C_H reflects a stable parabolic-like change with an $(C_{wf}/C_H)_{opt}$ value that enables the cycle to reach $P_{\max,3}$.
2. When f_H and f_L = 0.1 and T_{Lin} =400 K, the POW of the initial design plan is P=122.94 . When f_H, f_L, and f_R, and T_{Lin} are optimized and T_{Lin} =400 L, the maximum POW is $P_{\max}$=128.26 kW, with $P_{\max}$ increasing by about 4.33% compared to P. When further optimizing T_{Lin}, the double-maximum POW becomes $P_{\max,2}$=130.65kW, with $P_{\max,2}$ increasing by about 1.86% compared to $P_{\max}$ and by about 6.27% compared to P. When further optimizing C_{wf}/C_H, the triple-maximum POW becomes $P_{\max,3}$=137.40 kW, with $P_{\max,3}$ increasing by about 5.17% compared to $P_{\max,2}$, by about 7.13% compared to $P_{\max}$, and by about 11.76% compared to P.
3. When f_H, f_L, and f_R are optimized, increasing C_{wf} from 1.5 to 2.5 decreases $P_{\max,2}$ by about 5.82% and (T_{Lin}) $P_{\max,2}$ by about 3.50%, increases (η_{opt}) $P_{\max,2}$ by about 1.71%, decreases (f_{Hopt}) $P_{\max,2}$ by about 11.70%, and increases (f_{Ropt}) $P_{\max,2}$ by about 5.71% and (π_{opt}) $P_{\max,2}$ by about 5.49%. Increasing K_1 and K_2 from 0.1 to 0.3 increases $P_{\max,2}$ by about 24.83% and (T_{Lin}) $P_{\max,2}$ by about 0.89%, decreases (η_{opt}) $P_{\max,2}$ by about 0.426% and (f_{Hopt}) $P_{\max,2}$ by about 30.99%, increases (f_{Ropt}) $P_{\max,2}$ by about 23.21%, and decreases (η_{opt}) $P_{\max,2}$ by about 0.765%.
4. When f_H, f_L, f_R, T_{Lin} and C_{wf}/C_H are optimized, increasing C_L/C_H from 0.6 to 1.6 increases $P_{\max,3}$ by about 27.23% and $(C_{wf}/C_H)_{opt}$ by about 64%. Increasing K_1 from 0.2 to 0.4 increases $P_{\max,3}$ by about 6.12% and decreases $(C_{wf}/C_H)_{opt}$ by about 4.07%.
5. Using FTT to optimize the closed Brayton cycle for an SPP has obtained the optimal area distribution and optimal inlet temperature of the cooling fluid. The optimization results provide a theoretical basis for the design of a heat exchanger structure and for the selection of its temperature in a space-based power plant. Therefore, FTT is shown to be an important tool for studying SPPs.

ACKNOWLEDGEMENT

This work has been supported by the National Natural Science Foundation of China (Project Nos. 52171317 and 51779262) and the Graduate Innovative Fund of Wuhan Institute of Technology (Project No. CX2021043). The authors wish to thank the reviewers for their careful, unbiased, and constructive suggestions, which has led to this revised manuscript.

DATA AVAILABILITY STATEMENT

The published publication includes all graphics and data collected or developed during the study.

CONFLICT OF INTEREST

The author declared no potential conflicts of interest with respect to the research, authorship, and/or publication of this article.

ETHICS

There are no ethical issues with the publication of this manuscript.

FINANCIAL DISCLOSURE

The authors declared that this study has received no financial support.

REFERENCES

Andresen, B. (1983). *Finite-time thermodynamics*. University of Copenhagen.

Andresen, B., & Salamon, P. (2022). Future perspectives of finite-time thermodynamics. *Entropy, 24*(5), Article 690. [CrossRef]

Badescu, V. (2022). Maximum work rate extractable from energy fluxes. *Journal of Non-Equilibrium Thermodynamics, 47*(1), 77–93. [CrossRef]

Bejan, A. (1996). *Entropy generation minimization*. CRC Press.

Berry, R. S., Salamon, P., & Andresen, B. (2020). How it all began. *Entropy, 22*(8), Article 908. [CrossRef]

Chen, L. G., & Lorenzini, G. (2022a). Comparative performance for thermoelectric refrigerators with radiative and Newtonian heat transfer laws. Case Stud. *Thermal Engineering*, 34, Article 102069. [CrossRef]

Chen, L. G., Li, P. L., Xia, S. J., Kong, R., & Ge, Y. L. (2022b). Multi-objective optimization for membrane reactor for steam methane reforming heated by molten salt. *Scientific China: Technological Sciences, 65*(6), 1396–1414. [CrossRef]

Chen, L. G., Meng, F. K., Ge, Y. L., Feng, H. J., & Xia, S. J. (2020a). Performance optimization of a class of combined thermoelectric heating devices. *Science China: Technological Sciences, 63*(12), 2640–2648. [CrossRef]

Chen, L. G., Meng, F. K., Ge, Y. L., & Feng, H. J. (2021a). Performance optimization for a multielement thermoelectric refrigerator with another linear heat transfer law. *Journal of Non-Equilibrium Thermodynamics, 46*(2), 149–162. [CrossRef]

Chen, L. G., Qi, C. Z., Ge, Y. L., & Feng, H. J. (2022a). Thermal Brownian heat engine with external and internal irreversibilities. *Energy, 255*, Article 124582. [CrossRef]

Chen, L. G., Shi, S. S., Ge, Y. L., & Feng, H. J. (2023a). Performance of a generalized irreversible isothermal chemical pump with diffusive mass transfer law. *Energy, 263*(C), Article 125956. [CrossRef]

Chen, L. G., Shi, S. S., Feng, H. J., & Ge, Y. L. (2023b). Ecological optimization of an endoreversible three-mass-reservoir chemical pump. *Journal of Non-Equilibrium Thermodynamics, 48*. Article 62. [CrossRef]

Chen, L. G., Wu, C., & Sun, F. R. (1996). A generalized model of real heat engines and its performance. *Journal of the Energy Institute, 69*(481), 214–222.

Chen, L. G., Wu, C., & Sun, F. R. (1999). Finite time thermodynamic optimization or entropy generation minimization of energy systems. *Journal of Non-Equilibrium Thermodynamics, 24*(4), 327–359. [CrossRef]

Chen, L. G., & Xia, S. J. (2022a). Maximizing power output of endoreversible non-isothermal chemical engine via linear irreversible thermodynamics. *Energy, 255*, Article 124526. [CrossRef]

Chen, L. G., & Xia, S. J. (2022b). Minimizing entransy dissipation for heat transfer processes with $q \propto \Delta(T^n)$ and heat leakage. *Case Studies in Thermal Engineering, 36*, 102183. [CrossRef]

Chen, L. G., & Xia, S. J. (2022c). Heat engine cycle configurations for maximum work output with generalized models of reservoir thermal capacity and heat resistance. *Journal of Non-Equilibrium Thermodynamics, 47*(4), 329–338. [CrossRef]

Chen, L. G., & Xia, S. J. (2022d). Maximizing power of irreversible multistage chemical engine with linear mass transfer law using HJB theory. *Energy, 261*, Article 125277. [CrossRef]

Chen, L. G., & Xia, S. J. (2022e). Maximum work output configuration of finite potential source irreversible isothermal chemical engines with bypass mass leakage and mass resistance. *Energy Reports, 8*, 11440–11445. [CrossRef]

Chen, L. G., & Xia, S. J. (2022f). Maximum profit output configuration of multi-reservoir resource exchange intermediary. *Entropy, 24*(10), Article 1451. [CrossRef]

Chen, L. G., & Xia, S. J. (2023a). Power output and efficiency optimization of endoreversible non-isothermal chemical engine via Lewis analogy. *Scientific China: Technological Sciences, 66*, Article 45.

Chen, L. G., & Xia, S. J. (2023b). Power-optimization of multistage non-isothermal chemical engine system via Onsager equations, Hamilton-Jacobi-Bellman theory and dynamic programming. *Scientific China: Technological Sciences, 66*, 841–852. [CrossRef]

Chen, L. G., & Xia, S. J. (2023c). Maximum work configuration of finite potential source endoreversible non-isothermal chemical engines. *Journal of Non-Equilibrium Thermodynamics, 48*, 41–53. [CrossRef]

Chen, Y. R. (2011). Maximum profit configurations of commercial engines. *Entropy, 13*(6), 1137–1151. [CrossRef]

Curzon, F. L., & Ahlborn, B. (1975). Efficiency of a Carnot engine at maximum power output. *American Journal of Physics, 43*(1), 22–24. [CrossRef]

de Moura, E. F., Henriques, I. B., Guilherme, B., & Ribeiro, G. B. (2022b). Thermodynamic-dynamic coupling of a Stirling engine for space exploration. *Thermal Sciences and Engineering Progress, 32*, Article 101320. [CrossRef]

de Moura, E. F., Henriques, I. B., & Ribeiro, G. B. (2022a). Finite-time thermodynamics and exergy analysis of a Stirling engine for space power generation. *Thermal Sciences and Engineering Progress, 27*, Article 101078. [CrossRef]

Ding, Z. M., Qiu, S. S., Chen, L. G., & Wang, W. H. (2021). Modeling and performance optimization of double-resonance electronic cooling device with three electron reservoirs. *Journal of Non-Equilibrium Thermodynamics, 46*(3), 273–289. [CrossRef]

Ebrahimi, R. (2021). A new comparative study on performance of engine cycles under maximum thermal efficiency condition. *Energy Reports, 7*, 8858–8867. [CrossRef]

El-Genk, M. S., & Tournier, J. M. (2009). Performance analyses of VHTR plants with direct and indirect closed Brayton cycles and different working fluids. *Progress in Nuclear Energy, 51*(3), 556–572. [CrossRef]

Feidt, M. (2017). *Finite physical dimensions optimal thermodynamics: 1. Fundamentals*. ISTE Press and Elsevier. [CrossRef]

Feng, H. J., Qin, W. X., Chen, L. G., Cai, C. G., Ge, Y. L., & Xia, S. J. (2020). Power output, thermal efficiency and exergy-based ecological performance optimizations of an irreversible KCS-34 coupled to variable temperature heat reservoirs. *Energy Conversation and Management, 205*, Article 112424. [CrossRef]

Feng, H. J., Wu, Z. X., Chen, L. G., & Ge, Y. L. (2021). Constructal thermodynamic optimization for dual-pressure organic Rankine cycle in waste heat utilization system. *Energy Conversion and Management, 227*, Article 113585. [CrossRef]

Ge, Y. L., Chen, L. G., & Feng, H. J. (2021). Ecological optimization of an irreversible diesel cycle. *The European Physical Journal Plus, 136*(2), Article 198. [CrossRef]

Ge, Y. L., Shi, S. S., Chen, L. G., Zhang, D. F., & Feng, H. J. (2022). Power density analysis and multi-objective optimization for an irreversible dual cycle. *Journal of Non-Equilibrium Thermodynamics, 47*(3), 289–309. [CrossRef]

Gonca, G., & Sahin, B. (2016). Thermo-ecological performance analyses and optimizations of irreversible gas cycle engines. *Applied Thermal Engineering, 105*, 566–576. [CrossRef]

Gonca, G. (2017a). Exergetic and ecological performance analyses of a gas turbine system with two intercoolers and two re-heaters. *Energy, 124*, 579–588. [CrossRef]

Gonca, G. (2017b). Exergetic and thermo-ecological performance analysis of a gas-mercury combined turbine system (GMCTS). *Energy Conversion and Management, 151*, 32–42. [CrossRef]

Gonca, G. (2018). The effects of turbine design parameters on the thermo-ecologic performance of a regenerated gas turbine running with different fuel kinds. *Applied Thermal Engineering, 137*, 419–429. [CrossRef]

Gonca, G., & Başhan, V. (2019). Multi-criteria performance optimization and analysis of a gas-steam combined power system. *Journal of the Brazilian Society of Mechanical Sciences and Engineering, 41*(9), Article 373. [CrossRef]

Gonca, G., & Genc, I. (2019). Thermoecology-based performance simulation of a gas-mercury-steam power generation system (GMSPGS). *Energy Conversion and Management, 189*, 91–104. [CrossRef]

Gonca, G., & Guzel, B. (2022). Exergetic and exergo-economical analyses of a gas-steam combined cycle system. *Journal of Non-Equilibrium Thermodynamics, 47*(4), 415–431. [CrossRef]

Ibrahim, O. M., & Bourisli, R. I. (2021). The maximum power cycle operating between a heat source and heat sink with finite heat capacities. *Journal of Non-Equilibrium Thermodynamics, 46*(4), 383–402. [CrossRef]

Ibrahim, O. M., Klein, S. A., & Mitchell, J. W. (1991). Optimal heat power cycles for specified boundary conditions. *ASME: Journal of Engineering for Gas Turbines and Power, 113*(4), 514–521. [CrossRef]

Jin, Q. L., Xia, S. J., & Chen, L. G. (2023). A modified recompression S-CO2 Brayton cycle and its thermodynamic optimization. *Energy, 263*(E), Article 126015. [CrossRef]

Li, J., & Chen, L. G. (2021). Exergoeconomic performance optimization of space thermoradiative cell. *European Physical Journal Plus, 136*(6), Article 644. [CrossRef]

Li, J., & Chen, L. G. (2022). Optimal configuration of finite source heat engine cycle for maximum output work with complex heat transfer law. *Journal of Non-Equilibrium Thermodynamics, 47*(4), 433–441. [CrossRef]

Li, P. L., Chen, L. G., Xia, S. J., Kong, R., & Ge, Y. L. (2022). Total entropy generation rate minimization configuration of a membrane reactor of methanol synthesis via carbon dioxide hydrogenation. *Scientific China: Technological Sciences, 65*(3), 657–678. [CrossRef]

Lin, J., Xie, S., Jiang, C. X., Sun, Y. F., Chen, J. C., & Zhao, Y. R. (2022). Maximum power and corresponding efficiency of an irreversible blue heat engine for harnessing waste heat and salinity gradient energy. *Scientific China: Technological Sciences, 65*(3), 646–656. [CrossRef]

Liu, H. Q., Chi, Z. R., & Zang, S. S. (2020). Optimization of a closed Brayton cycle for space power systems. *Applied Thermal Engineering, 179*, Article 115611. [CrossRef]

Miao, X. Y., Zhang, H. C., Zhang, D., Zhang, C., & Huang, Z. (2022). Properties of nitrous oxide and helium mixtures for space nuclear recompression Brayton cycle. *Energy Reports, 8*, 2480–2489. [CrossRef]

Muschik, W., & Hoffmann, K. H. (2020). Modeling, simulation, and reconstruction of 2-reservoir heat-to-power processes in finite-time thermodynamics. *Entropy, 22*(9), Article 997. [CrossRef]

Park, H., & Kim, M. S. (2016). Performance analysis of sequential Carnot cycles with finite heat sources and heat sinks and its application in organic Rankine cycles. *Energy, 99*, 1–9. [CrossRef]

Paul, R., & Hoffmann K. H. (2022). Optimizing the piston paths of Stirling cycle cryocoolers. *Journal of Non-Equilibrium Thermodynamics, 47*(2), 195–203. [CrossRef]

Qi, C. Z., Ding, Z. M., Chen, L. G., Ge, Y. L., & Feng, H. J. (2021a). Modelling of irreversible two-stage combined thermal Brownian refrigerators and their optimal performance. *Journal of Non-Equilibrium Thermodynamics, 46*(2), 175–189. [CrossRef]

Qi, C. Z., Chen, L. G., Ding, Z. M., Ge, Y. L., & Feng, H. J. (2021b). A generalized irreversible thermal Brownian motor cycle and its optimal performance. *European Physical Journal Plus, 136*(11), Article 1120. [CrossRef]

Qi, C. Z., Chen, L. G., Ge, Y. L., & Feng, H. J. (2022a). Heat transfer effect on the performance of thermal Brownian refrigerator. *European Physical Journal Plus, 137*(3), Article 349. [CrossRef]

Qi, C. Z., Chen, L. G., Ge, Y. L., Yang, W. H., & Feng, H. J. (2022b). Thermal Brownian heat pump with external and internal irreversibilities. *European Physical Journal Plus, 137*(9), Article 1079. [CrossRef]

Qiu, S. S., Ding, Z. M., Chen, L. G., & Ge, Y. L. (2021a). Performance optimization of three-terminal energy selective electron generators. *Scientific China: Technical Sciences, 64*(8), 1641–1652. [CrossRef]

Qiu, S. S., Ding, Z. M., Chen, L. G., & Ge, Y. L. (2021b). Performance optimization of thermionic refrigerators based on van der Waals heterostructures. *Scientific China: Technological Sciences, 64*(5), 1007–1016. [CrossRef]

Qiu, X. F., Chen, L. G., Ge, Y. L., & Shi, S. S. (2022). Efficient power characteristic analyses and multi-objective optimization for an irreversible simple closed gas turbine cycle. *Entropy, 24*(11), Article 1531. [CrossRef]

Romano, L. F. R., & Ribeiro. G. B. (2021). Optimization of a heat pipe-radiator assembly coupled to a recuperated closed Brayton cycle for compact space power plants. *Applied Thermodynamic Engineering, 196*, Article 117355. [CrossRef]

Toro, C., & Lior, N. (2017). Analysis and comparison of solar-driven Stirling, Brayton and Rankine cycles for space power generation. *Energy, 120*, 549–564. [CrossRef]

Ust, Y., Sogut, O. S., Sahin, B., & Durmayaz, A. (2006). Ecological coefficient of performance (ECOP) optimization for an irreversible Brayton heat engine with variable-temperature thermal reservoirs. *Journal of the Energy Institute, 79*(1), 47–52. [CrossRef]

Valencia-Ortega, G., Levario-Medina, S., & Barranco-Jiménez, M. A. (2021). The role of internal irreversibilities in the performance and stability of power plant models working at maximum ϵ-ecological function. *Journal of Non-Equilibrium Thermodynamics, 46*(4), 413–429. [CrossRef]

Wang, C. L., Zhang, R., Guo, K. L., Zhang, D. L., Tian, W. X., Qiu, S. Z., & Su, G. H. (2021a). Dynamic simulation of a space gas-cooled reactor power system with a closed Brayton cycle. *Energy, 15*(4), 916–929. [CrossRef]

Wang, T., Chen, L. G., Liu, P., Ge, Y. L., & Feng, H. J. (2022). Performance analysis and optimization of an irreversible Carnot heat engine cycle for space power plant. *Energy Reports, 8*, 6593–6601. [CrossRef]

Wang, T., Ge, Y. L., Chen, L. G., Feng, H. J., & Yu, J. Y. (2021b). Optimal heat exchanger area distribution and low-temperature heat sink temperature for power optimization of an endoreversible space Carnot cycle. *Entropy, 23*(10), Article 1285. [CrossRef]

Wu, H., Ge, Y. L., Chen, L. G., & Feng, H. J. (2021). Power, efficiency, ecological function and ecological coefficient of performance optimizations of an irreversible Diesel cycle based on finite piston speed. *Energy, 216*, Article 119235. [CrossRef]

Wu, Z. X., Feng, H. J., Chen, L. G., Tang, W., Shi, J. C., & Ge, Y. L. (2020). Constructal thermodynamic optimization for ocean thermal energy conversion system with dual-pressure organic Rankine cycle. *Energy Conversion and Management, 210*(12), Article 112727. [CrossRef]

Wu, Z. X., Chen, L. G., Feng, H. J., & Ge, Y. L. (2021). Constructal thermodynamic optimization for a novel Kalina-organic Rankine combined cycle to utilize waste heat. *Energy Reports, 7*, 6095–6106. [CrossRef]

Xu, H. R., Chen, L. G., Ge, Y. L., & Feng, H. J. (2022). Multi-objective optimization of Stirling heat engine with various heat transfer and mechanical losses. *Energy, 256*, Article 124699. [CrossRef]

Zhang, H. C., Liu, X. T., Liu, J., & Li, Z. E. (2021). Characteristics and optimization of SCO2 Brayton cycle system for power sodium-cooled fast reactor on Mars. *Thermal Science, 25*(6B), 4659–4666. [CrossRef]

Zhang, X., Yang, G. F., Yan, M. Q., Ang, L. K., Ang, Y. S., & Chen, J. C. (2021). Design of an all-day electrical power generator based on thermoradiative devices. *Science China: Technological Sciences, 64*(10), 2166–2173. [CrossRef]